Autophagy regulates sphingolipid levels in the liver[S]

Aikaterini Alexaki,* Sita D. Gupta,[†] Saurav Majumder,* Mari Kono,* Galina Tuymetova,* Jeffrey M. Harmon,[§] Teresa M. Dunn,[†] and Richard L. Proia[1,*]

Genetics of Development and Disease Branch,* National Institute of Diabetes and Digestive and Kidney Diseases, National Institutes of Health, Bethesda, MD 20892; and Departments of Biochemistry[†] and Molecular Biology and Pharmacology,[§] Uniformed Services University of the Health Sciences, Bethesda, MD 20184

Abstract Sphingolipid levels are tightly regulated to maintain cellular homeostasis. During pathologic conditions such as in aging, inflammation, and metabolic and neurodegenerative diseases, levels of some sphingolipids, including the bioactive metabolite ceramide, are elevated. Sphingolipid metabolism has been linked to autophagy, a critical catabolic process in both normal cell function and disease; however, the in vivo relevance of the interaction is not well-understood. Here, we show that blocking autophagy in the liver by deletion of the *Atg7* gene, which is essential for autophagosome formation, causes an increase in sphingolipid metabolites including ceramide. We also show that overexpression of serine palmitoyltransferase to elevate de novo sphingolipid biosynthesis induces autophagy in the liver. The results reveal autophagy as a process that limits excessive ceramide levels and that is induced by excessive elevation of de novo sphingolipid synthesis in the liver.[jlr] Dysfunctional autophagy may be an underlying mechanism causing elevations in ceramide that may contribute to pathogenesis in diseases.—Alexaki, A., S. D. Gupta, S. Majumder, M. Kono, G. Tuymetova, J. M. Harmon, T. M. Dunn, and R. L. Proia. **Autophagy regulates sphingolipid levels in the liver. *J. Lipid Res*. 2014.** 55: **2521–2531.**

Supplementary key words ceramide • lipids • endoplasmic reticulum • triglycerides • lipophagy

Sphingolipids are a structurally and functionally diverse family of lipids that serve as membrane components and signaling molecules (1, 2). In the endoplasmic reticulum (ER), serine palmitoyltransferase (SPT) catalyzes the first and rate-limiting step of de novo sphingolipid biosynthesis with the condensation of serine and palmitoyl-CoA to form a sphingoid base that is eventually converted to ceramide, a key sphingolipid that occupies a central hub in the metabolic pathway (3). Ceramide undergoes anabolic reactions to generate sphingomyelin and various glycosphingolipids, or catabolic reactions, which lead to the generation of sphingosine and sphingosine-1-phosphate (S1P).

Alterations in ceramide metabolism have been implicated in many pathophysiologies, including aging (4–6), neurodegeneration (7, 8), metabolic diseases (9–15), cancer (16–20), and stress responses (5). However, the mechanisms that regulate cellular ceramide levels under physiologic and pathophysiologic conditions are still not well-understood.

Changes in the levels of ceramide and other sphingolipid metabolites have been shown to affect macroautophagy (referred to hereafter as autophagy) in a variety of cell types (21–27). Autophagy is a catabolic process that starts with the generation of a double-membrane cup-like phagophore from the ER or other sources (28, 29); the phagophore then captures cellular material and matures into an autophagosome that will subsequently fuse with a lysosome to form an autolysosome, enabling degradation of the engulfed material. This process is crucial for removal of pathogens and damaged proteins and organelles, as well as for the reutilization of nutrients to generate energy and maintain homeostasis. Clearance of toxic or defective cellular components protects from degenerative, metabolic, and inflammatory diseases (30). Some forms of autophagy are specific, uniquely targeting mitochondria (mitophagy) (31), segments of the ER (ER-phagy or reticulophagy) (32), or triglyceride stores (lipophagy) (33) for degradation. Impaired autophagy is encountered, along with increased ceramide levels, in a number of pathophysiologic conditions, including aging (34, 35), neurodegeneration (36, 37), obesity (10), and type 2 diabetes (9).

This research was supported by the Intramural Research Program of the National Institutes of Health, National Institute of Diabetes and Digestive and Kidney Diseases, the USU Grant CO75PI and National Institutes of Health Grants R01NS072446 and R21HD080181, the Lipidomics Shared Resource, Hollings Cancer Center, Medical University of South Carolina (P30 CA138313), and the Lipidomics Core in the South Carolina Lipidomics and Pathobiology COBRE (P20 RR017677).

Manuscript received 11 June 2014 and in revised form 10 October 2014.

Published, JLR Papers in Press, October 20, 2014
DOI 10.1194/jlr.M051862

Abbreviations: ER, endoplasmic reticulum; DAPI, 4',6-diamidino-2-phenylindole; fSPT, fusion serine palmitoyltransferase; GFP, green fluorescent protein; Mut-fSPT, mutant fusion palmitoyl transferase; ORO, Oil Red O; PFU, plaque forming units; S1P, sphingosine-1-phosphate; SPT, serine palmitoyltransferase.

[1]To whom correspondence should be addressed.
e-mail: richardp@intra.niddk.nih.gov

[S] The online version of this article (available at http://www.jlr.org) contains supplementary data in the form of five figures.

In this study, we have addressed the function of autophagy in controlling sphingolipid levels in the liver, an organ system where autophagy serves critical functions in maintaining homeostasis and preventing metabolic disease (38–40). We have found that when autophagy is genetically blocked in the liver, several sphingolipid species, including ceramide, increase substantially. To determine whether elevations in SPT activity in liver can, in turn, trigger autophagy, we expressed the SPT holoenzyme for the first time in vivo, enabling direct initiation of de novo sphingolipid biosynthesis. We found that the elevated SPT activity with concomitant sphingolipid synthesis induces autophagy in the liver. The results demonstrate that autophagy controls sphingolipid levels in vivo and suggests the possibility that dysfunctional autophagy in numerous pathologic conditions may cause alterations in sphingolipid homeostasis.

MATERIALS AND METHODS

Plasmid and adenoviral construction

The construction of the fusion SPT (fSPT) gene has previously been described, as has the mutant fSPT (Mut-fSPT) gene that was used as a control (41). fSPT was inserted in the multiple cloning site of the dual-CCM and the dual green fluorescent protein (GFP)-CCM vectors (Vector BioLabs). Construction of the adenovirus vectors, incorporation into the human adenovirus serotype 5 (DE1/E3), amplification of the virus stock, and CsCl amplification were performed by Vector BioLabs to generate the fSPT-, fSPT-GFP-, Mut-fSPT-, and null-adenoviruses.

Mice and infections

Wild-type C57BL6 mice were purchased from the mouse repository at NCI, Frederick, MD. All mice used throughout the study were on a C57BL6 background. GFP-LC3$^{+/+}$ (42) and Atg7$^{lox/lox}$ (43) mice were kindly provided by Masaaki Komatsu and Dr. Noboru Mizushima, respectively. Atg7$^{lox/lox}$ mice were bred with Mx-cre and Alb-cre mice to generate the Atg7-indKO (Atg7$^{lox/lox}$ Mx-cre) and Atg7LKO (Atg7$^{loxl/lox}$ Alb-cre) mice, respectively. Atg7-indKO mice were injected after weaning with 300 μl poly(I:C) solution (1 mg/ml in water) three times at 48 h intervals, as previously described (43), to induce Cre expression and harvested 3 weeks after the last injection. C57BL6 mice, GFP-LC3$^{+/+}$ transgenic mice, and Atg7LKO mice (with their controls) were used at around 7–10 weeks of age. PCR with mouse-tail DNA was used to determine the genotype of the GFP-LC3, Atg7^{lox}, and Cre loci; primers and conditions for all PCRs have been previously described (42, 44). Mice were infected with a tail-vein injection of 5×10^8 plaque forming units (PFU) of fSPT-adenovirus (or Mut-fSPT-adenovirus) to generate the low-dose model and with 5×10^9 PFU of the same viruses to generate the high-dose model. Mice were fed a regular chow diet [or a high-fat diet (60% kcal fat, Research Diets, Inc.) when indicated]. All animal procedures were approved by the National Institute of Diabetes and Digestive and Kidney Diseases Animal Care and Use Committee and were performed in accordance with the National Institutes of Health guidelines.

Microsome preparation and in vitro SPT activity

Microsomes were prepared from liver as previously described (45). Microsomal SPT activity was assayed by measuring acyl-CoA-dependent incorporation of [^{3}H]serine into long-chain bases as previously described (46).

Immunoblotting

Microsome preparations from the livers of the adenovirus-injected mice were used for immunoblotting with the anti-sptlc1 (BD Biosciences) antibody. Total liver homogenate was used for all other immunoblotting experiments. Liver was homogenized in RIPA buffer (Boston BioProducts) with protease inhibitors (Thermo Scientific), crude liver homogenate centrifuged at 8,000 *g*, and the resulting supernatant stored at −80°C. A PVDF membrane was used when immunoblotting with anti-LC3B (Sigma-Aldrich); nitrocellulose membranes were used in all other cases. Chemiluminescence detection was used when analyzing samples from SPT-adenovirus-injected mice; when analyzing samples from Atg7indKO, Atg7LKO, and *Atg7*$^{lox/lox}$ mice, the LI-COR Odyssey system was used.

Lipid analysis

Mass spectrometry. Sphingolipids in plasma and liver homogenates were measured by high-performance liquid chromatography-tandem mass spectrometry by the Lipidomics Core at the Medical University of South Carolina on a Thermo Finnigan TSQ 7000 triple quadrupole mass spectrometer, operating in a multiple reaction monitoring-positive ionization mode as described (47).

Triglyceride assay. Liver was homogenized in PBS and protein content was measured with the BCA protein assay (Thermo Scientific). Lipids were extracted using chloroform/methanol (2:1), dried overnight, and resuspended in isopropanol. Triglyceride content was measured with triglyceride reagent (Pointe Scientific, Inc.).

Microscopy

Mice were perfused with 4% paraformaldehyde. Fixed liver tissue was embedded in OCT medium. Oil Red O (ORO) staining was performed by Histoserv, Inc. Sections were examined on a Leica DMLB microscope. For confocal microscopy, 8 μm-thick liver sections were cut from tissue embedded in OCT medium. Sections were fixed again in 4% paraformaldehyde and counterstained with 4',6-diamidino-2-phenylindole (DAPI). Sections were examined in a LSM 5 Live Duoscan (Zeiss) confocal microscope and analyzed with Zen 2009 software. For electron microscopy, liver tissue was fixed with 1% glutaraldehyde/4% paraformaldehyde at 4°C for 24 h. Further processing was performed by JFE Enterprises. Sections were examined with an electron microscope (Philips EM 410).

Quantitative PCR

Total RNA from mouse liver was purified using the RNeasy mini kit (Qiagen). Total RNA (1 μg) was first digested with DNase I and subsequently reverse-transcribed with the SuperScript First-Strand synthesis system (Invitrogen) by following the manufacturer's instructions. Expression levels of mRNA were determined by using predesigned assay-on-demand probes and primers (Applied Biosystems) on an ABI Prism 7700 sequence detection system (Applied Biosystems).

Statistical analysis

Unpaired Student's *t*-tests were performed to compare results between different groups. $P < 0.05$ was considered statistically significant.

RESULTS

Autophagy regulates sphingolipid levels

We sought to determine whether autophagy regulates sphingolipid levels by using mice with an inducible deletion

of *Atg7*, a gene essential for autophagosome formation. In these autophagy-defective mice (Atg7-indKO, having the genotype $Atg^{lox/lox}$ Mx-cre), the *Atg7* gene is deleted in multiple tissues in adult mice, including the liver, by stimulation of Cre recombinase expression through administration of poly(I:C) (42).

Sphingolipid levels were quantified in the liver of autophagy-defective (Atg7-indKO) and control ($Atg7^{lox/lox}$) mice. Mass spectrometry analysis was performed to determine the levels of ceramide, dihydroceramide, sphingosine, dihydrosphingosine, S1P, and dihydro-S1P. Compared with control mice, the autophagy-defective mice showed a significant increase in their total liver ceramide levels, as well as those of several individual ceramide species (**Fig. 1A**). Dihydrosphingosine, dihydroceramide, and sphingosine levels were also increased in the livers of the autophagy-defective mice (Fig. 1A). These results indicate that autophagy has a major role in limiting sphingolipid metabolites including ceramide in the liver.

To investigate whether SPT, the enzyme that initiates de novo sphingolipid biosynthesis, was increased, we determined protein levels of Sptlc1 and Sptlc2. Immunoblot analysis demonstrated a substantial increase in the levels of Sptlc1 and Sptlc2 subunits in the livers of autophagy-defective mice compared with the livers from control mice (Fig. 1B). SPT enzymatic activity was also significantly increased in the livers of autophagy-defective mice compared with livers from control mice (Fig. 1C). Sptlc1 mRNA levels were not increased in livers of autophagy-defective mice compared with the livers from control mice (Fig. 1D), indicating that altered transcriptional regulation of Sptlc1 did not contribute to increased SPT activity. Interestingly,

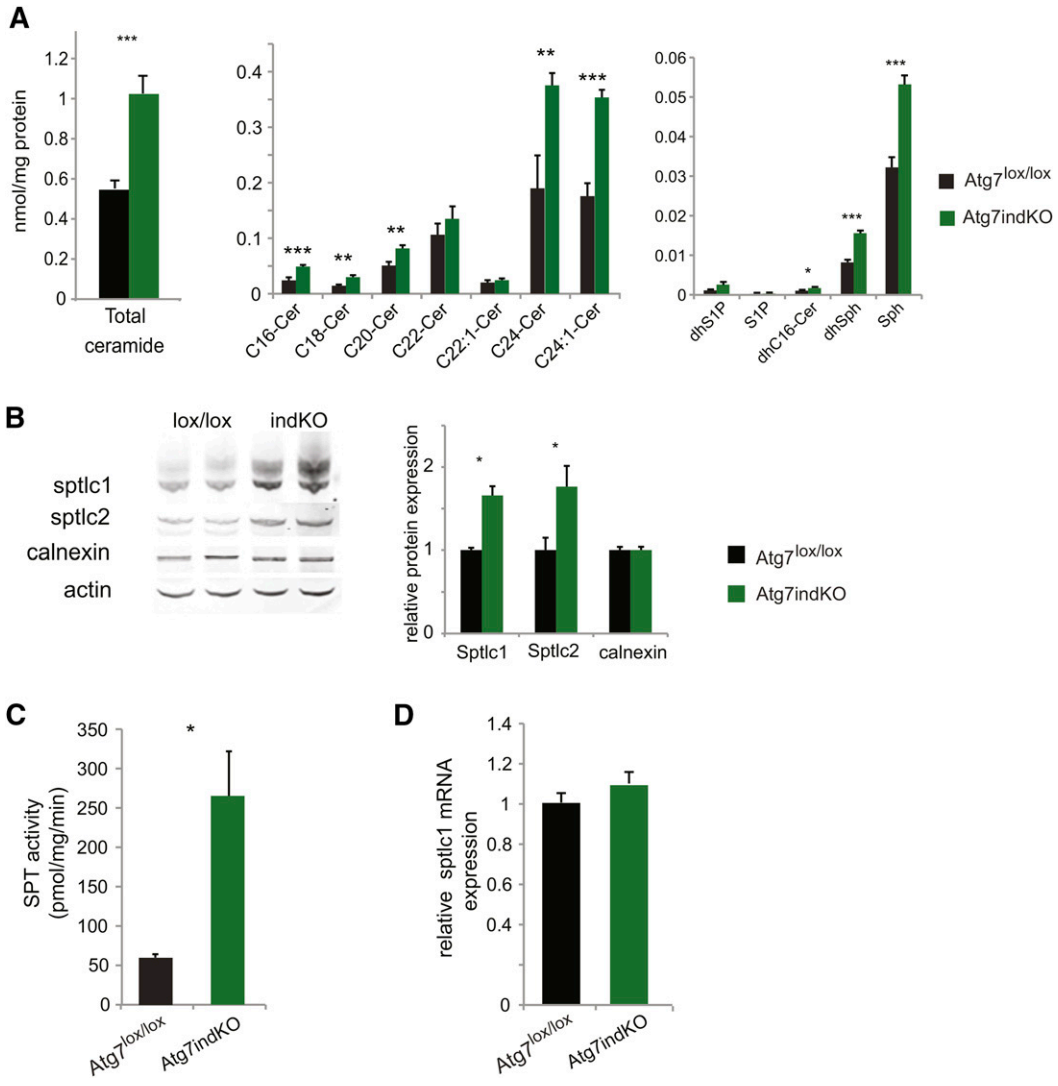

Fig. 1. Deletion of *Atg7* increases ceramide and SPT levels in the liver. Liver homogenates from Atg7-indKO and control ($Atg7^{lox/lox}$) mice were used to measure sphingolipid concentration (A) and for immunoblotting, with quantitation of the bands. Actin was used as a loading control (B). Microsomal membranes were isolated and used to perform SPT assays (C). RNA was isolated and used for quantitative PCR analysis (D). Data for individual ceramide species, protein expression, SPT activity, and mRNA expression are presented as mean (±SEM) ($Atg7^{lox/lox}$ n = 6, Atg7indKO n = 5; $*P < 0.05$, $**P < 0.01$, $***P < 0.001$). Cer, ceramide; dhC16-Cer, dihydro-C16-ceramide; dhS1P, dihydrosphingosine-1-phosphate; Sph, sphingosine;

unlike the protein subunits of SPT, calnexin, another resident protein of the ER, was not increased in the livers of the autophagy-defective mice compared with the livers from control mice (Fig. 1B), suggesting an autophagy-specific effect toward SPT.

To confirm that the changes in sphingolipid metabolism seen with the Atg7-indKO mouse were not secondary to an extrahepatic effect of autophagy, we conducted the same experiments described above with another line of mice with a solely liver-specific deletion of *Atg7* (Atg7LKO) using Cre recombinase driven by the albumen promoter. The Atg7LKO mice, having the genotype, $Atg^{lox/lox}$ albumen-Cre recapitulated all the results that were seen with the Atg7-indKO mice (supplementary Fig. I) including the substantial increase in ceramide levels. Collectively, these results show that a block in hepatic autophagy has a large impact on sphingolipid metabolism in the liver.

In vivo SPT overexpression

We sought to determine whether elevation of the sphingolipid metabolic pathway was a positive regulator of autophagy in the liver. SPT is a heterotrimer consisting of two large subunits (SPTLC1 and SPTLC2 or its functional isoform SPTLC3) and one small subunit (ssSPT isoforms a or b). To facilitate the expression of an active SPT enzyme in vivo, a fSPT gene, which contained the human subunits SPTLC1, SPTLC2, and ssSPTa as a single in-frame polypeptide chain (SPTLC2-ssSPTa-SPTLC1), was utilized (**Fig. 2A**). The fSPT protein, which had previously been shown to have catalytic activity similar to the wild-type enzyme (41, 48), was incorporated into an adenovirus (fSPT-adenovirus). A point mutation in the catalytic site of the fusion SPT (Mut-fSPT) that leads to inactivation of the enzyme (49) was used to generate a control adenovirus (Mut-fSPT-adenovirus). A second control adenovirus with no SPT gene (null-adenovirus) was also used. Intravenous injection of the adenoviruses was used for liver-directed expression (Fig. 2A).

Induction of liver SPT activity and sphingolipid metabolites with fSPT-adenovirus

We evaluated induction of SPT expression in the liver of C57BL6 mice using two doses of fSPT-adenovirus [low dose: 5×10^8 plaque-forming units (PFU)/mouse; high dose: 5×10^9 PFU/mouse] by immunoblotting and detection of enzymatic activity. Immunoblotting was performed with an antibody to SPTCL1, which reacts with both fSPT and endogenous mouse Sptlc1. fSPT protein was very highly expressed relative to the endogenous Sptlc1 in the livers of mice injected with the highest dose of virus (Fig. 2B). Correspondingly, the level of SPT activity was 12-fold higher in liver microsomes isolated from the high-dose fSPT-adenovirus-injected mice compared with liver microsomes of control-adenovirus-injected mice (Fig. 2C). At the low dose, the fSPT protein was readily detectable at day 3 and its expression levels progressively increased until day 10; on day 14, fSPT protein levels substantially declined (Fig. 2D). The protein-expression data correlated with SPT enzymatic activity (Fig. 2E), which showed a 3-fold increase over control on day 10 and a decline on day 14.

Mass spectrometry analysis was performed to determine the levels of ceramide, dihydroceramide, sphingosine, dihydrosphingosine, S1P, and dihydro-S1P in the liver and plasma of mice 24 h after administration of the high-dose fSPT-adenovirus. Most of the ceramide species were substantially increased by this treatment; total ceramide was increased by 2-fold and 3.5-fold in the liver and plasma, respectively (**Fig. 3A, B**). A large increase was observed for dihydrosphingosine and dihydroceramide both in the liver and in the plasma. These sphingolipids are generated during the initial steps of de novo sphingolipid biosynthesis, before ceramide formation, and an increase in their concentrations is consistent with increased flux of substrate

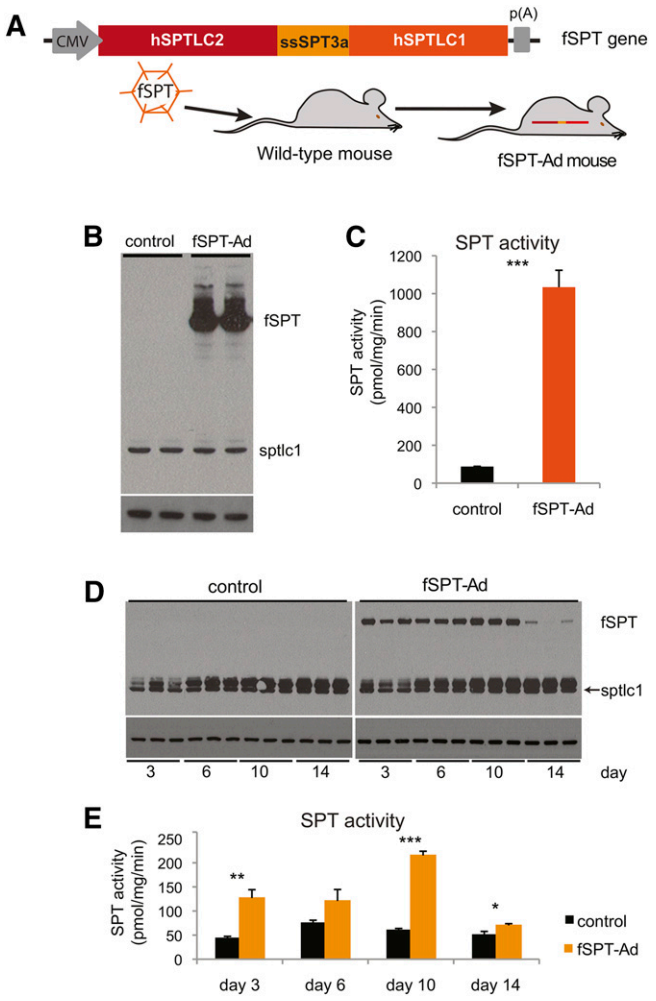

Fig. 2. In vivo expression of fSPT. A schematic of the fSPT gene is shown. The fSPT gene was cloned into the adenoviral genome and delivered to the liver through an iv injection (A). Mice were injected with 5×10^9 PFU (high dose) of fSPT-adenovirus (fSPT-Ad) or control adenovirus, livers were harvested at 24 h, and microsomal membranes were isolated and used for immunoblotting (B) and SPT assay (C). Mice were injected with 5×10^8 PFU (low dose) of fSPT-Ad or control adenovirus, livers were harvested on day 3, 6, 10, or 14, and microsomal membranes were isolated and used for immunoblotting (D) and SPT assay (E). The control adenovirus used was the null-adenovirus. The band running immediately above sptlc1 in (D) is nonspecific. Calnexin is used as a loading control. SPT activity data are presented as mean (±SEM) (n = 3; $*P < 0.05$, $**P < 0.01$, $***P < 0.001$).

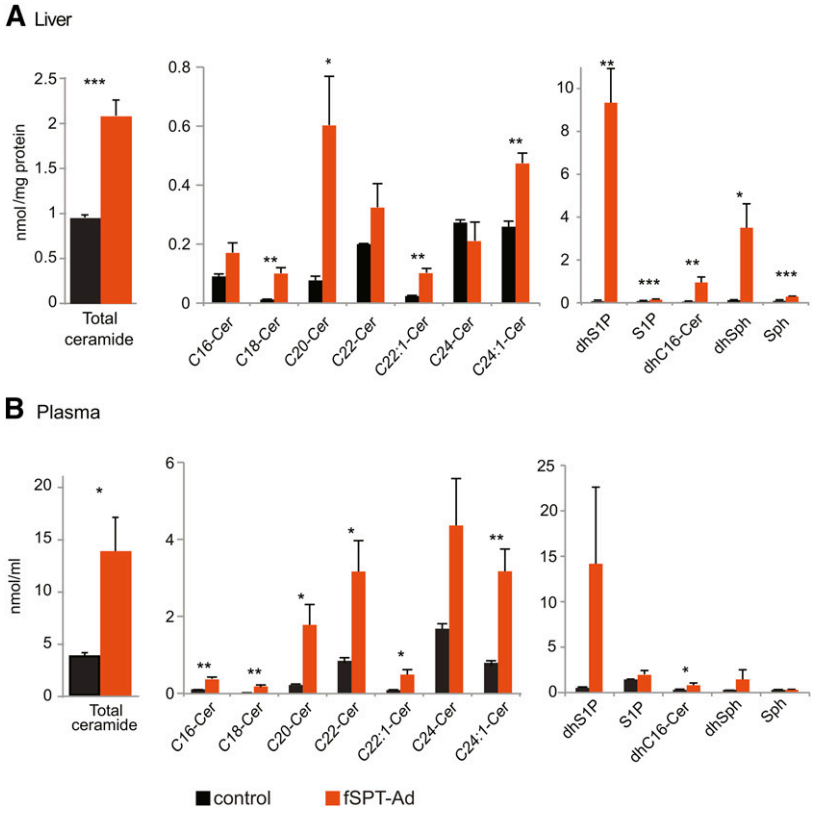

Fig. 3. Sphingolipid levels following high-dose fSPT-adenovirus administration. Mice were injected with the high dose (5×10^9 PFU) of fSPT-adenovirus (fSPT-Ad) or control adenovirus, and livers and blood were harvested at 24 h. Concentrations of ceramide species with different fatty acid chain lengths, and of dihydrosphingosine-1-phosphate (dhS1P), S1P, dihydro-C16-ceramide (dhC16-Cer), dihydrosphingosine (dhSph) and sphingosine (Sph) are shown in liver homogenates (A) and plasma (B). The control adenovirus used was the null-adenovirus. Data for individual ceramide species are presented as mean (±SEM) (n = 4; $*P < 0.05$, $**P < 0.01$, $***P < 0.001$). Cer, ceramide.

through the de novo pathway. Sphingosine and S1P, which are generated further down the pathway by degradation of ceramide, were significantly increased in the liver but not in the plasma (Fig. 3A, B).

In the mice treated with the low dose of fSPT-adenovirus, several species of ceramide were increased in the liver, albeit to a lower extent compared with the high dose. Total ceramide levels were increased both at day 3 and day 10, and to approximately the same extent (19% and 22%, respectively) (**Fig. 4A, B**). Increases were also observed in dihydrosphingosine and dihydroceramide, consistent with increased de novo sphingolipid biosynthesis (Fig. 4A, B). In the plasma, the increases in sphingolipid metabolites in the fSPT-adenovirus-injected mice were, for the most part, not statistically significant (supplementary Fig. IIA, B).

Administration of the high dose of fSPT-adenovirus produced highly elevated serum levels of alanine aminotransferase and aspartate aminotransferase compared with treatment with the control adenovirus, indicating active fSPT expression caused liver damage (supplementary Fig. IIIA). In contrast, serum alanine aminotransferase and aspartate aminotransferase levels were not significantly changed after administration of the lower dose of fSPT-adenovirus relative to treatment with the same dose of a control virus (supplementary Fig. IIIA). The relative extent of infection in the liver was monitored by the expression of an fSPT-containing adenovirus that also expressed GFP from a separate promoter. The high dose of this virus produced GFP expression to a much greater extent and intensity in liver cells than the low dose (supplementary Fig. IIIC).

The high dose of fSPT-adenovirus caused lethality in the majority of the mice within 32 h postinjection (supplementary Fig. IIIB). However, at 24 h, the hepatocytes showed little evidence of apoptosis by deoxynucleotidyl transferase dUTP nick end labeling (TUNEL) assays (supplementary Fig. IV). The same dose of a control virus (Mut-fSPT-adenovirus or null-adenovirus) was not lethal over a 1 week observation period (data not shown). In contrast to the lethality seen with the high dose of fSPT-adenovirus, the 10-fold lower dose of fSPT-adenovirus was well-tolerated, with mice showing no apparent signs of adverse reaction.

The results demonstrated that robust SPT activity in the liver could be generated from the fSPT protein, leading to elevations of sphingolipid metabolites in both liver and plasma. The results also showed that at high levels of SPT activity, liver toxicity occurred, which provided a dramatic illustration of the necessity for tight regulation of the pathway (50).

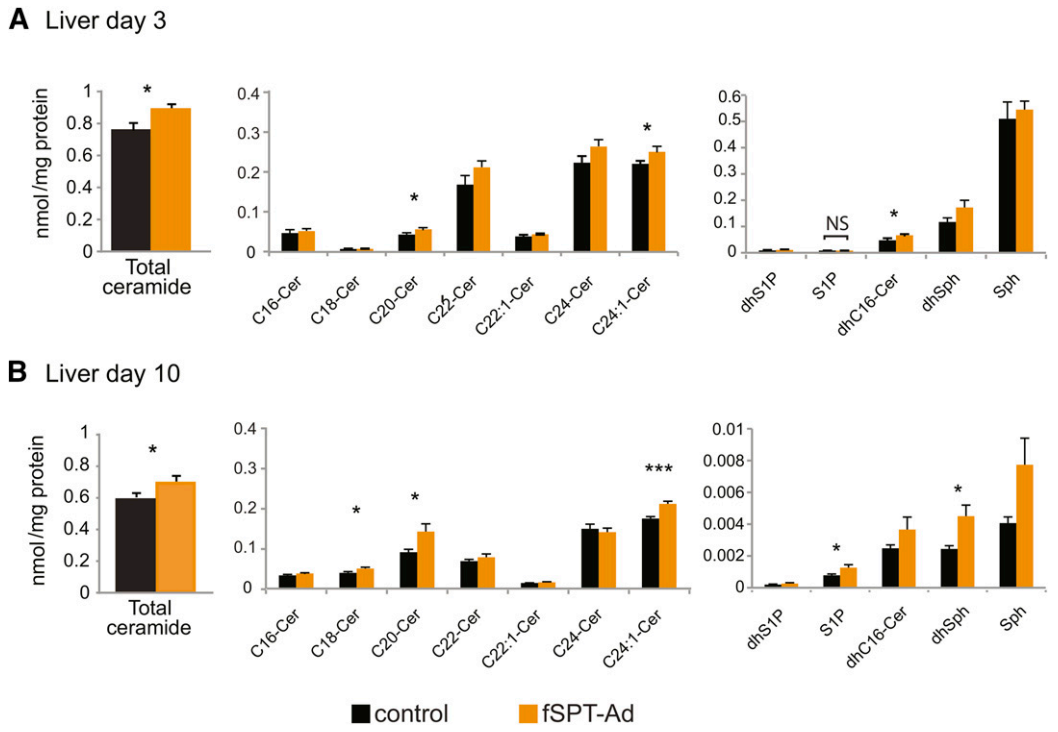

Fig. 4. Sphingolipid levels in the liver following low-dose fSPT-adenovirus administration. Mice were injected with the low dose (5×10^8 PFU) of fSPT-adenovirus (fSPT-Ad) or control adenovirus, and livers were harvested on day 3 (A) or day 10 (B). The control adenovirus used was the null-adenovirus. Concentrations of sphingolipids are shown in liver homogenates. Data for individual ceramide species are presented as mean (±SEM) (n = 7; $*P < 0.05$, $**P < 0.01$, $***P < 0.001$). Cer, ceramide; dhC16-Cer, dihydro-C16-ceramide; dhS1P, dihydrosphingosine-1-phosphate; Sph, sphingosine;

Increased SPT activity leads to an upregulation of autophagy

Having established an effective means to elevate SPT activity in the liver and initiate de novo sphingolipid biosynthesis, we sought to determine whether increased SPT activity leads to an upregulation of autophagy in the liver. We utilized GFP-LC3$^{+/+}$ transgenic mice, in which the autophagic process can be visualized in tissues by the characteristic appearance of GFP-LC3-positive puncta, representing autophagosomes (43). Administration of both the high dose and low dose of fSPT-adenovirus led to a marked increase of GFP-LC3 puncta (**Fig. 5A**). The high dose caused the appearance of substantial GFP-LC3 puncta at day 1 (24 h). Induction of GFP-LC3 puncta with the lower dose of fSPT-adenovirus was observed at day 3. Immunoblot analysis of liver extracts confirmed that fSPT expression stimulated the conversion of the nonlipidated form of LC3 (LC3-I) to the lipidated form (LC3-II) (Fig. 5B) that is associated with the membranes of autophagosomes. However, the expression of fSPT did not alter the levels of Atg7.

Electron-microscopy analysis was performed to gain insight into the autophagic process that was occurring in the mice with elevated SPT activity. Livers from mice receiving the high dose of fSPT-adenovirus [at 24 h, when little apoptosis was detectable (supplementary Fig. IV)] showed dramatic changes, with the most striking being the appearance within hepatocytes of atypically large vacuoles that contained several types of structures and organelles (**Fig. 6Ai, ii**), multiple membranous concentric structures (Fig. 6Aiii), abundant autophagophore-like structures (Fig. 6Aiv), and lipid droplets extensively associated with membranous structures (Fig. 6Av).

In mice receiving the low dose of fSPT-adenovirus, hepatocytes had a normal appearance (Fig. 6Bi), nevertheless, autophagosomes were frequently observed, and demonstrated a more classical appearance than the autophagosomes observed with the high dose of fSPT-adenovirus (Fig. 6Bii, iii). Small lipid droplets were often included within autophagosomes (Fig. 6Biv), and several large lipid droplets contained multiple membranes (Fig. 6Bv), both of which are characteristic signs of lipophagy (33), the autophagy of lipid droplets, a process where autophagosomes deliver triglycerides to lysosomes for degradation.

Because of the ultrastructural evidence of autophagy of lipid droplets in fSTP-adenovirus-treated mice, we next sought to determine if the increase in de novo sphingolipid biosynthesis initiated by SPT had an effect on hepatic triglyceride degradation, a pathway that involves lysosomal function during autophagy (33). Obese mice, which store excess triglycerides in the liver, were injected with either a low dose of fSPT-adenovirus or a control adenovirus. Three days after the injections, ORO staining in liver sections and triglyceride measurements in liver homogenates revealed significantly reduced lipid levels in the livers of SPT-overexpressing mice compared with the livers from control mice (Fig. 6C, D). These results are

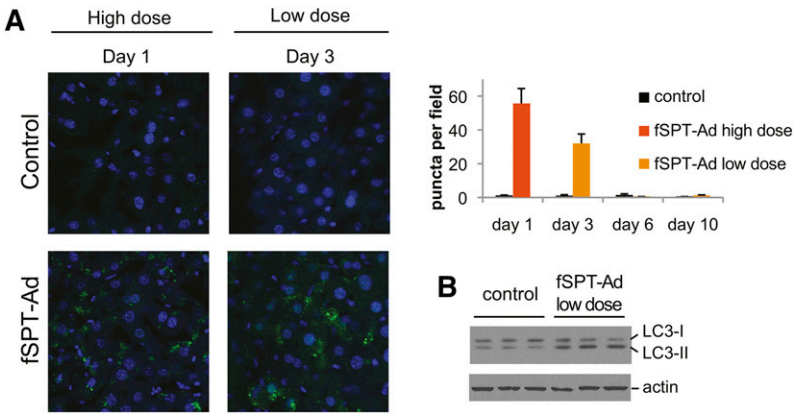

Fig. 5. SPT expression upregulates autophagy in the liver. GFP-LC3$^{+/+}$ mice were injected with high (5×10^9 PFU) or low (5×10^8 PFU) dose of fSPT-adenovirus (fSPT-Ad) or Mut-fSPT-adenovirus (control). Mice injected with the high dose were perfused with 4% paraformaldehyde (24 h) after injection; mice injected with the low dose were perfused 3 days after injection. Liver sections were examined by confocal microscopy. The GFP-LC3 puncta per field were counted and the mean (±SEM) of eight fields is shown for each treatment (A). Wild-type mice were injected with a low dose (5×10^8 PFU) of fSPT-Ad or Mut-fSPT-adenovirus (control). Livers were harvested 3 days after injection. Immunoblotting was performed on liver homogenates (B). Actin was used as a loading control.

consistent with the conclusion that excessive de novo sphingolipid synthesis drives autophagy-dependent triglyceride degradation.

DISCUSSION

Sphingolipid metabolism must be tightly regulated to maintain proper amounts of complex sphingolipids in membranes and to control levels of highly bioactive intermediates such as ceramide and S1P. The regulatory mechanisms that operate to control sphingolipid metabolism are only now beginning to be understood (1). Here we describe autophagy as a mechanism to regulate sphingolipid levels in vivo (**Fig. 7**).

Mice deficient in the expression of *Atg7*, a gene required for autophagosome biogenesis, had highly elevated ceramide levels in the liver. Such an increase in ceramide could be the result of a block in the degradation of ceramide, increased de novo biosynthesis, and/or increased recycling of complex sphingolipids. The finding that SPT protein and activity are highly elevated in the liver of *Atg7*-KO mice is consistent with an increase in the flux of substrate though the de novo pathway, providing a mechanism to explain the increased dihydrosphinglipids which were also present. Other effects of autophagy on the sphingolipid metabolic pathway are likely, including a direct role in degrading ceramides, which may be incorporated as components of the autophagosome membrane (25).

How can autophagy regulate SPT activity? Normal mRNA levels of Sptlc1 in the livers of autophagy-defective mice suggest that the regulation is not the result of a transcriptional response to a block in autophagy. Neither does it seem to be due to a generalized block in autophagy of the ER, as the SPT subunits are enriched relative to the ER protein calnexin in the *Atg7*-defective mice. Instead, our results may be consistent with a selective ER autophagy mechanism that targets SPT specifically. A selective autophagic process termed "ER-phagy" or "reticulophagy," in which damaged or excess ER formed in response to aggregated proteins is removed, has previously been described (51). A similar mechanism may regulate SPT levels through direct autophagic targeting of the protein subunits or ER membranes containing excessive ceramide in the proximity of SPT. During the process of ER-phagy, delimiting membranes of autophagosomes are derived from the ER itself and contain characteristic multilamellar structures (32).

Several studies have implicated the sphingolipid metabolic pathway in autophagy through direct addition of sphingolipids (21, 52), the use of inhibitors of metabolism (either chemical or genetic) (24), and by indirect activation of de novo biosynthesis (17, 25, 53, 54). In our study, we asked if initiation of de novo sphingolipid biosynthesis alone, in the absence of other stimuli, could directly activate autophagy in the liver, an organ where autophagy has been shown to be critical for maintaining normal homeostasis and preventing metabolic disease (38). We found that when SPT activity was elevated, even marginally, autophagosome formation was dramatically increased. With high levels of SPT activity, remarkably abundant multilamellar membranes surrounded by autophagophore-like structures were observed. To some extent, these may resemble karmelae structures (55). Potentially, the SPT protein may be involved in their formation (56), or they may be due to increased autophagy flux, as they also bear similarity to the concentric membranous structures that are generated when there is a downstream block in autophagy (42). Because autophagy has been shown to modulate the mobilization of cellular lipid stores in the liver, a process often termed macrolipophagy or lipophagy (33, 57), we assessed the levels of hepatic triglycerides as a functional correlate of autophagy. Triglyceride stores were reduced after autophagy induction by increased SPT expression. Electron microscopy revealed autophagosome-like structures associated with lipid droplets when de novo sphingolipid biosynthesis was elevated. The results are consistent with the conclusion that functional autophagy is greatly stimulated by elevated SPT activity (Fig. 7).

Although the exact means of how increased sphingolipid metobolism regulates autophagy is not well-understood, many studies have pointed to direct signaling by ceramide as a mechanism to stimulate autophagy (reviewed elsewhere) (17, 53, 58–60). In particular, ceramide has been shown to induce autophagy via direct anchoring of autophagosomes to mitochondria (21), through downregulation

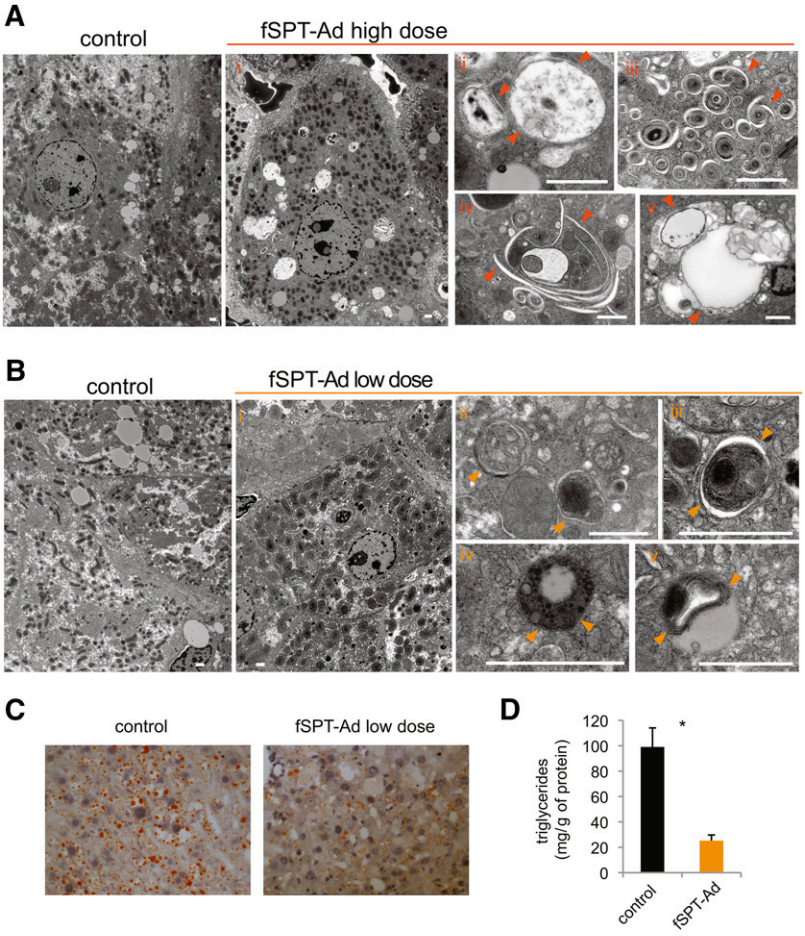

Fig. 6. Ultrastructural analysis after autophagy upregulation by SPT. A: Mice were injected with a high dose (5×10^9 PFU) of fSPT-adenovirus (fSPT-Ad) or null-adenovirus (control) and livers harvested at 24 h. Electron micrographs of liver tissue represent: low-power (i) and high-power (ii) magnification showing abnormally large vacuoles; multiple membranous concentric structures (iii); multiple autophagophores (iv); and lipid droplets extensively associated with membranes (v). B: Mice were injected with a low dose (5×10^8 PFU) of fSPT-Ad or null-adenovirus (control) and harvested on day 3. Electron micrographs of liver tissue represent: low-power magnification showing normal hepatocyte appearance (i); typical autophagosomes (ii, iii); autophagosome containing lipid droplets (iv); and lipid droplets associated with multiple membranes (iv). Arrowheads point to double membranes. The scale bar indicates 1 μm. C: C57BL6 mice that had been on a high-fat diet for eight weeks (obese mice) were injected with a low dose (5×10^8 PFU) of fSPT-Ad or null-adenovirus (control). Livers were harvested 3 days after injection. Frozen liver sections were stained with ORO. D: Triglyceride concentration was assayed on liver homogenates from the same mice. Data are presented as mean (±SEM) (n = 5; $^*P < 0.05$).

of nutrient transporters (23, 61), as well as through disruption of the Beclin-Bcl-2 complex (24). It has also been suggested that de novo sphingolipid biosynthesis might supply the ceramides that are vital for the formation of the autophagosome membranes derived from the ER, thus stimulating autophagosome formation (25). Ceramides with fatty acid chain lengths of 20 and longer were elevated by induction of de novo sphingolipid synthesis in the liver, indicating that ceramide synthase 2 and possibly ceramide synthase 4 were involved in their production (2). The levels of the ceramides with C22–24 fatty acids, synthesized by ceramide synthase 2, are critical for proper membrane function and homeostasis in liver (62–64). An imbalance in their levels may induce autophagy.

S1P has also been shown to induce autophagy by both intracellular and extracellular mechanisms. Depletion of S1P phosphohydrolase-1, an enzyme that dephosphorylates intracellular S1P, triggers ER-stress-induced autophagy because of the increased intracellular S1P levels (65). Extracellular S1P, acting through the cell surface receptor, S1P5, has been shown to induce autophagy in prostate cancer cells, possibly as a mechanism that promotes cell survival (66).

The initiation of de novo sphingolipid biosynthesis has been difficult to study in isolation because of an inability to directly express SPT, the first committed enzyme in sphingolipid biosynthesis. The full subunit structure of SPT was only recently recognized with the identification of the small subunit SPT, which is required along with two different large subunits for full SPT activity. The demonstration that a fusion of the two large subunits (SPTLC1 and SPTLC2) with one small subunit (ssSPTa)

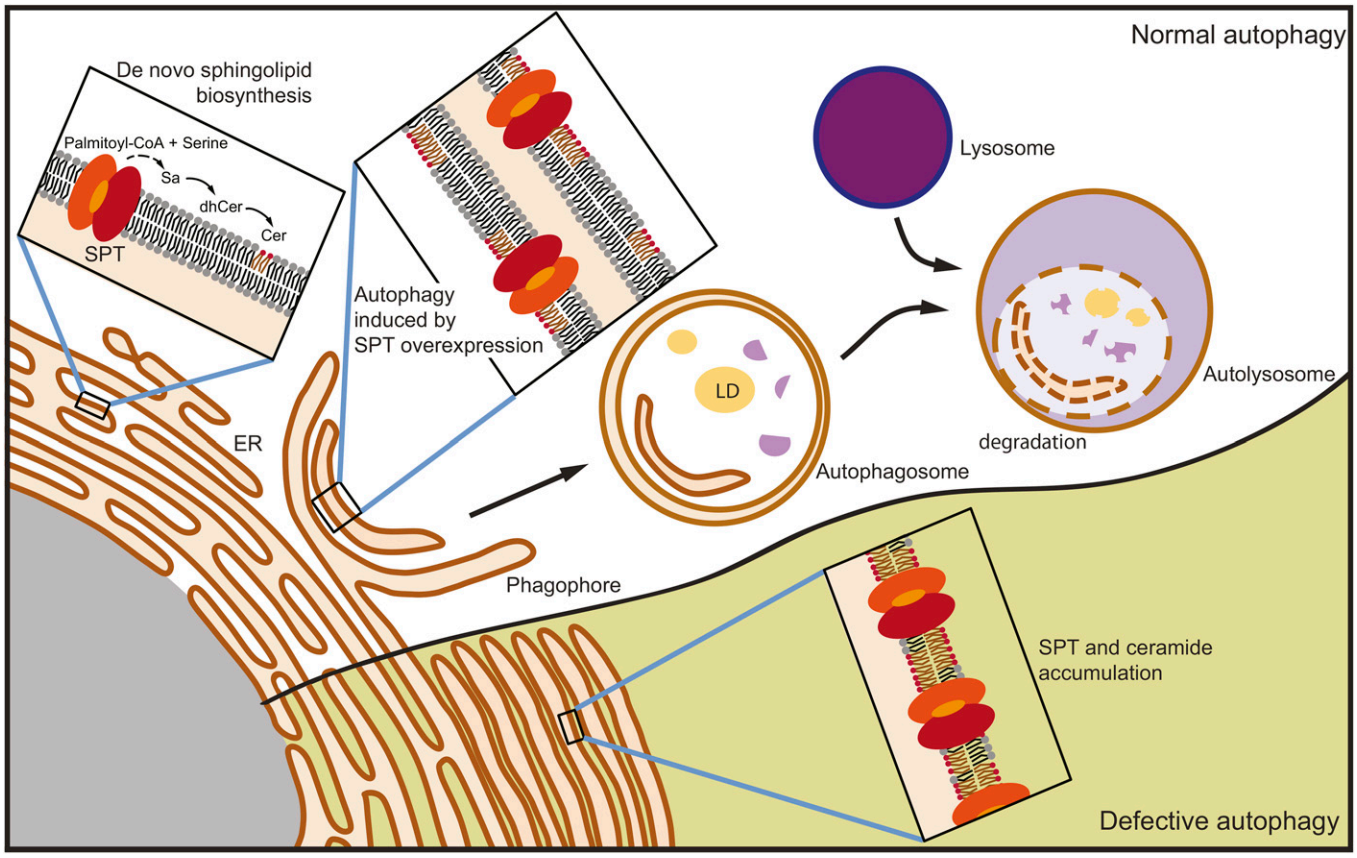

Fig. 7. Model of the regulation of sphingolipid metabolism by autophagy. De novo sphingolipid biosynthesis takes place in the ER, initiated by SPT, and results in the production of ceramide, a metabolite that is normally transferred out of the ER. In the absence of efficient autophagy, both ceramide and SPT become elevated within the ER. In this model ceramide levels are restrained by autophagy of ER membranes enriched in ceramide and SPT. LD, lipid droplet.

gives rise to a fully catalytically active SPT (41, 48) has enabled us to express the active enzyme in the liver of mice and to determine its direct effects on autophagy. This is the first in vivo model to achieve robust elevation of SPT activity by direct genetic manipulation. Earlier studies of de novo sphingolipid biosynthesis initiation relied on secondary stimuli (such as lipopolysaccharide and chemical agents) to activate SPT, which likely activate other pathways and are thus difficult to harness for in vivo studies.

The finding that ceramide levels rise when autophagy is blocked has potentially important implications for human disease. Elevations in ceramide levels have been linked as a pathogenic factor to a number of conditions, including obesity (10), diabetes (9), neurodegeneration (36, 37), and aging (34, 35). All of these conditions have been associated with dysfunctional autophagy (67). Our data are consistent with the possibility that an impairment in autophagy may lead to elevations of cellular ceramide, which in turn may disturb signaling cascades involved in their pathogenesis.

The authors thank Laura Allende for helping with revisions to the manuscript. They also thank Noboru Mizushima and Masaaki Komatsu for kindly providing the LC3-GFP and Atg7$^{lox/lox}$ mice, respectively.

REFERENCES

1. Breslow, D. K., and J. S. Weissman. 2010. Membranes in balance: mechanisms of sphingolipid homeostasis. *Mol. Cell.* **40:** 267–279.
2. Merrill, A. H., Jr. 2011. Sphingolipid and glycosphingolipid metabolic pathways in the era of sphingolipidomics. *Chem. Rev.* **111:** 6387–6422.
3. Hannun, Y. A., and L. M. Obeid. 2002. The ceramide-centric universe of lipid-mediated cell regulation: stress encounters of the lipid kind. *J. Biol. Chem.* **277:** 25847–25850.
4. Huang, X., B. R. Withers, and R. C. Dickson. 2014. Sphingolipids and lifespan regulation. *Biochim. Biophys. Acta.* **1841:** 657–664.
5. Nikolova-Karakashian, M. N., and K. A. Rozenova. 2010. Ceramide in stress response. *Adv. Exp. Med. Biol.* **688:** 86–108.
6. Obeid, L. M., and Y. A. Hannun. 2003. Ceramide, stress, and a "LAG" in aging. *Sci. SAGE KE.* **2003:** PE27.
7. Ben-David, O., and A. H. Futerman. 2010. The role of the ceramide acyl chain length in neurodegeneration: involvement of ceramide synthases. *Neuromolecular Med.* **12:** 341–350.
8. Cutler, R. G., J. Kelly, K. Storie, W. A. Pedersen, A. Tammara, K. Hatanpaa, J. C. Troncoso, and M. P. Mattson. 2004. Involvement of oxidative stress-induced abnormalities in ceramide and cholesterol metabolism in brain aging and Alzheimer's disease. *Proc. Natl. Acad. Sci. USA.* **101:** 2070–2075.
9. Chavez, J. A., and S. A. Summers. 2012. A ceramide-centric view of insulin resistance. *Cell Metab.* **15:** 585–594.
10. Samad, F., L. Badeanlou, C. Shah, and G. Yang. 2011. Adipose tissue and ceramide biosynthesis in the pathogenesis of obesity. *Adv. Exp. Med. Biol.* **721:** 67–86.
11. Bikman, B. T., and S. A. Summers. 2011. Ceramides as modulators of cellular and whole-body metabolism. *J. Clin. Invest.* **121:** 4222–4230.
12. Hla, T., and A. J. Dannenberg. 2012. Sphingolipid signaling in metabolic disorders. *Cell Metab.* **16:** 420–434.

13. Holland, W. L., J. T. Brozinick, L. P. Wang, E. D. Hawkins, K. M. Sargent, Y. Liu, K. Narra, K. L. Hoehn, T. A. Knotts, A. Siesky, et al. 2007. Inhibition of ceramide synthesis ameliorates glucocorticoid-, saturated-fat-, and obesity-induced insulin resistance. *Cell Metab.* **5:** 167–179.
14. Holland, W. L., and S. A. Summers. 2008. Sphingolipids, insulin resistance, and metabolic disease: new insights from in vivo manipulation of sphingolipid metabolism. *Endocr. Rev.* **29:** 381–402.
15. Holland, W. L., B. T. Bikman, L. P. Wang, G. Yuguang, K. M. Sargent, S. Bulchand, T. A. Knotts, G. Shui, D. J. Clegg, M. R. Wenk, et al. 2011. Lipid-induced insulin resistance mediated by the proinflammatory receptor TLR4 requires saturated fatty acid-induced ceramide biosynthesis in mice. *J. Clin. Invest.* **121:** 1858–1870.
16. Truman, J. P., M. Garcia-Barros, L. M. Obeid, and Y. A. Hannun. 2014. Evolving concepts in cancer therapy through targeting sphingolipid metabolism. *Biochim. Biophys. Acta.* **184:** 1174–1188.
17. Jiang, W., and B. Ogretmen. 2014. Autophagy paradox and ceramide. *Biochim. Biophys. Acta.* **1841:** 783–792.
18. Morad, S. A., and M. C. Cabot. 2013. Ceramide-orchestrated signalling in cancer cells. *Nat. Rev. Cancer.* **13:** 51–65.
19. Ryland, L. K., T. E. Fox, X. Liu, T. P. Loughran, and M. Kester. 2011. Dysregulation of sphingolipid metabolism in cancer. *Cancer Biol. Ther.* **11:** 138–149.
20. Saddoughi, S. A., and B. Ogretmen. 2013. Diverse functions of ceramide in cancer cell death and proliferation. *Adv. Cancer Res.* **117:** 37–58.
21. Sentelle, R. D., C. E. Senkal, W. Jiang, S. Ponnusamy, S. Gencer, S. P. Selvam, V. K. Ramshesh, Y. K. Peterson, J. J. Lemasters, Z. M. Szulc, et al. 2012. Ceramide targets autophagosomes to mitochondria and induces lethal mitophagy. *Nat. Chem. Biol.* **8:** 831–838.
22. Pattingre, S., C. Bauvy, S. Carpentier, T. Levade, B. Levine, and P. Codogno. 2009. Role of JNK1-dependent Bcl-2 phosphorylation in ceramide-induced macroautophagy. *J. Biol. Chem.* **284:** 2719–2728.
23. Peralta, E. R., and A. L. Edinger. 2009. Ceramide-induced starvation triggers homeostatic autophagy. *Autophagy.* **5:** 407–409.
24. Scarlatti, F., C. Bauvy, A. Ventruti, G. Sala, F. Cluzeaud, A. Vandewalle, R. Ghidoni, and P. Codogno. 2004. Ceramide-mediated macroautophagy involves inhibition of protein kinase B and up-regulation of beclin 1. *J. Biol. Chem.* **279:** 18384–18391.
25. Sims, K., C. A. Haynes, S. Kelly, J. C. Allegood, E. Wang, A. Momin, M. Leipelt, D. Reichart, C. K. Glass, M. C. Sullards, et al. 2010. Kdo2-lipid A, a TLR4-specific agonist, induces de novo sphingolipid biosynthesis in RAW264.7 macrophages, which is essential for induction of autophagy. *J. Biol. Chem.* **285:** 38568–38579.
26. Spassieva, S. D., T. D. Mullen, D. M. Townsend, and L. M. Obeid. 2009. Disruption of ceramide synthesis by CerS2 down-regulation leads to autophagy and the unfolded protein response. *Biochem. J.* **424:** 273–283.
27. Xiong, Y., H. J. Lee, B. Mariko, Y. C. Lu, A. J. Dannenberg, A. S. Haka, F. R. Maxfield, E. Camerer, R. L. Proia, and T. Hla. 2013. Sphingosine kinases are not required for inflammatory responses in macrophages. *J. Biol. Chem.* **288:** 32563–32573.
28. Ge, L., D. Melville, M. Zhang, and R. Schekman. 2013. The ER-Golgi intermediate compartment is a key membrane source for the LC3 lipidation step of autophagosome biogenesis. *eLife.* **2:** e00947.
29. Tooze, S. A., and T. Yoshimori. 2010. The origin of the autophagosomal membrane. *Nat. Cell Biol.* **12:** 831–835.
30. Rubinsztein, D. C., P. Codogno, and B. Levine. 2012. Autophagy modulation as a potential therapeutic target for diverse diseases. *Nat. Rev. Drug Discov.* **11:** 709–730.
31. Ashrafi, G., and T. L. Schwarz. 2013. The pathways of mitophagy for quality control and clearance of mitochondria. *Cell Death Differ.* **20:** 31–42.
32. Bernales, S., S. Schuck, and P. Walter. 2007. ER-phagy: selective autophagy of the endoplasmic reticulum. *Autophagy.* **3:** 285–287.
33. Singh, R., S. Kaushik, Y. Wang, Y. Xiang, I. Novak, M. Komatsu, K. Tanaka, A. M. Cuervo, and M. J. Czaja. 2009. Autophagy regulates lipid metabolism. *Nature.* **458:** 1131–1135.
34. Molano, A., Z. Huang, M. G. Marko, A. Azzi, D. Wu, E. Wang, S. L. Kelly, A. H. Merrill, Jr., S. C. Bunnell, and S. N. Meydani. 2012. Age-dependent changes in the sphingolipid composition of mouse CD4+ T cell membranes and immune synapses implicate glucosylceramides in age-related T cell dysfunction. *PLoS ONE.* **7:** e47650.
35. Rivas, D. A., E. P. Morris, P. H. Haran, E. P. Pasha, S. Morais Mda, G. G. Dolnikowski, E. M. Phillips, and R. A. Fielding. 2012. Increased ceramide content and NFκB signaling may contribute to the attenuation of anabolic signaling after resistance exercise in aged males. *J. Appl. Physiol.* **113:** 1727–1736.
36. Arboleda, G., L. C. Morales, B. Benitez, and H. Arboleda. 2009. Regulation of ceramide-induced neuronal death: cell metabolism meets neurodegeneration. *Brain Res. Rev.* **59:** 333–346.
37. de la Monte, S. M. 2012. Triangulated mal-signaling in Alzheimer's disease: roles of neurotoxic ceramides, ER stress, and insulin resistance reviewed. *J. Alzheimers Dis.* **30(Suppl 2):** S231–S249.
38. Schneider, J. L., and A. M. Cuervo. 2014. Liver autophagy: much more than just taking out the trash. *Nat. Rev. Gastroenterol. Hepatol.* **11:** 187–200.
39. Yang, L., P. Li, S. Fu, E. S. Calay, and G. S. Hotamisligil. 2010. Defective hepatic autophagy in obesity promotes ER stress and causes insulin resistance. *Cell Metab.* **11:** 467–478.
40. Zhang, C., and A. M. Cuervo. 2008. Restoration of chaperone-mediated autophagy in aging liver improves cellular maintenance and hepatic function. *Nat. Med.* **14:** 959–965.
41. Gable, K., S. D. Gupta, G. Han, S. Niranjanakumari, J. M. Harmon, and T. M. Dunn. 2010. A disease-causing mutation in the active site of serine palmitoyltransferase causes catalytic promiscuity. *J. Biol. Chem.* **285:** 22846–22852.
42. Komatsu, M., S. Waguri, T. Ueno, J. Iwata, S. Murata, I. Tanida, J. Ezaki, N. Mizushima, Y. Ohsumi, Y. Uchiyama, et al. 2005. Impairment of starvation-induced and constitutive autophagy in Atg7-deficient mice. *J. Cell Biol.* **169:** 425–434.
43. Mizushima, N., A. Yamamoto, M. Matsui, T. Yoshimori, and Y. Ohsumi. 2004. In vivo analysis of autophagy in response to nutrient starvation using transgenic mice expressing a fluorescent autophagosome marker. *Mol. Biol. Cell.* **15:** 1101–1111.
44. Mizushima, N. 2009. Methods for monitoring autophagy using GFP-LC3 transgenic mice. *Methods Enzymol.* **452:** 13–23.
45. Han, G., K. Gable, L. Yan, M. Natarajan, J. Krishnamurthy, S. D. Gupta, A. Borovitskaya, J. M. Harmon, and T. M. Dunn. 2004. The topology of the Lcb1p subunit of yeast serine palmitoyltransferase. *J. Biol. Chem.* **279:** 53707–53716.
46. Han, G., S. D. Gupta, K. Gable, S. Niranjanakumari, P. Moitra, F. Eichler, R. H. Brown, Jr., J. M. Harmon, and T. M. Dunn. 2009. Identification of small subunits of mammalian serine palmitoyltransferase that confer distinct acyl-CoA substrate specificities. *Proc. Natl. Acad. Sci. USA.* **106:** 8186–8191.
47. Pettus, B. J., J. Bielawski, A. M. Porcelli, D. L. Reames, K. R. Johnson, J. Morrow, C. E. Chalfant, L. M. Obeid, and Y. A. Hannun. 2003. The sphingosine kinase 1/sphingosine-1-phosphate pathway mediates COX-2 induction and PGE2 production in response to TNF-alpha. *FASEB J.* **17:** 1411–1421.
48. Harmon, J. M., D. Bacikova, K. Gable, S. D. Gupta, G. Han, N. Sengupta, N. Somashekarappa, and T. M. Dunn. 2013. Topological and functional characterization of the ssSPTs, small activating subunits of serine palmitoyltransferase. *J. Biol. Chem.* **288:** 10144–10153.
49. Gable, K., G. Han, E. Monaghan, D. Bacikova, M. Natarajan, R. Williams, and T. M. Dunn. 2002. Mutations in the yeast LCB1 and LCB2 genes, including those corresponding to the hereditary sensory neuropathy type I mutations, dominantly inactivate serine palmitoyltransferase. *J. Biol. Chem.* **277:** 10194–10200.
50. Merrill, A. H., Jr. 2002. De novo sphingolipid biosynthesis: a necessary, but dangerous, pathway. *J. Biol. Chem.* **277:** 25843–25846.
51. Bernales, S., K. L. McDonald, and P. Walter. 2006. Autophagy counterbalances endoplasmic reticulum expansion during the unfolded protein response. *PLoS Biol.* **4:** e423.
52. Daido, S., T. Kanzawa, A. Yamamoto, H. Takeuchi, Y. Kondo, and S. Kondo. 2004. Pivotal role of the cell death factor BNIP3 in ceramide-induced autophagic cell death in malignant glioma cells. *Cancer Res.* **64:** 4286–4293.
53. Young, M. M., M. Kester, and H. G. Wang. 2013. Sphingolipids: regulators of crosstalk between apoptosis and autophagy. *J. Lipid Res.* **54:** 5–19.
54. Russo, S. B., C. F. Baicu, A. Van Laer, T. Geng, H. Kasiganesan, M. R. Zile, and L. A. Cowart. 2012. Ceramide synthase 5 mediates lipid-induced autophagy and hypertrophy in cardiomyocytes. *J. Clin. Invest.* **122:** 3919–3930.
55. Wright, R., M. Basson, L. D'Ari, and J. Rine. 1988. Increased amounts of HMG-CoA reductase induce "karmellae": a proliferation of stacked membrane pairs surrounding the yeast nucleus. *J. Cell Biol.* **107:** 101–114.
56. Snapp, E. L., R. S. Hegde, M. Francolini, F. Lombardo, S. Colombo, E. Pedrazzini, N. Borgese, and J. Lippincott-Schwartz. 2003.

Formation of stacked ER cisternae by low affinity protein interactions. *J. Cell Biol.* **163:** 257–269.
57. Singh, R., and A. M. Cuervo. 2012. Lipophagy: connecting autophagy and lipid metabolism. *Int. J. Cell Biol.* **2012:** 282041.
58. Bedia, C., T. Levade, and P. Codogno. 2011. Regulation of autophagy by sphingolipids. *Anticancer. Agents Med. Chem.* **11:** 844–853.
59. Lavieu, G., F. Scarlatti, G. Sala, T. Levade, R. Ghidoni, J. Botti, and P. Codogno. 2007. Is autophagy the key mechanism by which the sphingolipid rheostat controls the cell fate decision? *Autophagy.* **3:** 45–47.
60. Zheng, W., J. Kollmeyer, H. Symolon, A. Momin, E. Munter, E. Wang, S. Kelly, J. C. Allegood, Y. Liu, Q. Peng, et al. 2006. Ceramides and other bioactive sphingolipid backbones in health and disease: lipidomic analysis, metabolism and roles in membrane structure, dynamics, signaling and autophagy. *Biochim. Biophys. Acta.* **1758:** 1864–1884.
61. Guenther, G. G., E. R. Peralta, K. R. Rosales, S. Y. Wong, L. J. Siskind, and A. L. Edinger. 2008. Ceramide starves cells to death by downregulating nutrient transporter proteins. *Proc. Natl. Acad. Sci. USA.* **105:** 17402–17407.
62. Pewzner-Jung, Y., O. Brenner, S. Braun, E. L. Laviad, S. Ben-Dor, E. Feldmesser, S. Horn-Saban, D. Amann-Zalcenstein, C. Raanan, T. Berkutzki, et al. 2010. A critical role for ceramide synthase 2 in liver homeostasis: II. Insights into molecular changes leading to hepatopathy. *J. Biol. Chem.* **285:** 10911–10923.
63. Pewzner-Jung, Y., H. Park, E. L. Laviad, L. C. Silva, S. Lahiri, J. Stiban, R. Erez-Roman, B. Brugger, T. Sachsenheimer, F. Wieland, et al. 2010. A critical role for ceramide synthase 2 in liver homeostasis: I. Alterations in lipid metabolic pathways. *J. Biol. Chem.* **285:** 10902–10910.
64. Silva, L. C., O. Ben David, Y. Pewzner-Jung, E. L. Laviad, J. Stiban, S. Bandyopadhyay, A. H. Merrill, Jr., M. Prieto, and A. H. Futerman. 2012. Ablation of ceramide synthase 2 strongly affects biophysical properties of membranes. *J. Lipid Res.* **53:** 430–436.
65. Lépine, S., J. C. Allegood, Y. Edmonds, S. Milstien, and S. Spiegel. 2011. Autophagy induced by deficiency of sphingosine-1-phosphate phosphohydrolase 1 is switched to apoptosis by calpain-mediated autophagy-related gene 5 (Atg5) cleavage. *J. Biol. Chem.* **286:** 44380–44390.
66. Chang, C. L., M. C. Ho, P. H. Lee, C. Y. Hsu, W. P. Huang, and H. Lee. 2009. S1P(5) is required for sphingosine 1-phosphate-induced autophagy in human prostate cancer PC-3 cells. *Am. J. Physiol. Cell Physiol.* **297:** C451–C458.
67. Choi, A. M., S. W. Ryter, and B. Levine. 2013. Autophagy in human health and disease. *N. Engl. J. Med.* **368:** 1845–1846.